IEEE Access
Multidisciplinary ⋮ Rapid Review ⋮ Open Access Journal

Received 6 May 2024, accepted 2 June 2024, date of publication 10 June 2024, date of current version 18 June 2024.

Digital Object Identifier 10.1109/ACCESS.2024.3411781

RESEARCH ARTICLE

A Triple Noise Tolerant Zeroing Neural Network for Time-Varing Matrix Inverse

FEIXIANG YANG AND YUN HUANG
College of Computer Science and Engineering, Jishou University, Jishou 416000, China
Corresponding author: Yun Huang (huangyun@jsu.edu.cn)

This work was supported in part by the National Natural Science Foundation of China under Grant 62062036, Grant 62066015, and Grant 62006095; and in part by the College Students' Innovation Training Center Project at Jishou University under Grant JDCX20231012.

ABSTRACT Matrix inversion is a fundamental operation utilized across numerous disciplines such as mathematics, engineering, and control theory. The original zeroing neural network (OZNN) method has proven effective in tackling the challenge of time-varying matrix inversion (TVMI) under ideal conditions. The integration-enhanced zeroing neural network (IEZNN) is commonly used to handle TVMI issues in the presence of various types of noise. In this paper, we have enhanced the IEZNN model's tolerance to noise by introducing a dual integral component, resulting in the dual noise tolerant zeroing neural network (DNTZNN) model. We have further improved this model by incorporating a positive odd activation function to create the triple noise tolerant zeroing neural network (TNTZNN). This advancement enables the TNTZNN to effectively solve TVMI problems despite various noise disturbances. Consequently, the TNTZNN model demonstrates excellent convergence and robustness even under noisy conditions. Furthermore, theoretical analysis grounded on the Lyapunov theorem validates the convergence and resilience of the TNTZNN model against diverse forms of noise. Computational simulations further substantiate the superior efficacy of the proposed TNTZNN model in resolving TVMI problems.

INDEX TERMS Activation function, matrix inverse, noise tolerant, time-variant problems, zeroing neural network, double integral.

I. INTRODUCTION

The task of matrix inversion is a common occurrence in mathematical disciplines, control theory, and is utilized across several critical domains such as chaotic systems [1], [2], image processing [3], [4], robotic kinematics [5], [6], [7], [8], and beyond. Hence, the development of more efficient methods for addressing the matrix inversion problem is of utmost significance.

Typical computational methodologies can be broadly divided into two categories. One category encompasses serial numerical techniques, such as the Newton-Raphson iteration [9], [10], whose computational complexity increases proportionally with the matrix's dimensionality. As the matrix dimension grows, computational tasks become increasingly challenging. Conversely, parallel neural network-based methodologies circumvent this limitation and are amenable to hardware implementation. Notable neural network approaches include gradient neural networks (GNN) [11], [12] and recurrent neural networks (RNN) [7], [13]. These methods have been employed to address static matrix inversion problems. However, when confronted with time-varying matrix inversion tasks, they struggle to achieve real-time tracking of the theoretical solution due to lag errors, thereby resorting to approximate solutions instead.

To address this challenge, Zhang et al. introduced a zeroing neural network (ZNN) [14]. What sets this network apart from the previously mentioned methods is its capacity to leverage temporal derivative information from the matrix. This capability allows the ZNN to counteract lag errors, consequently empowering it to tackle time-varying matrix inversion (TVMI) problems.

In the past two decades, a multitude of researchers have employed various ingenious techniques to optimize, enhance,

The associate editor coordinating the review of this manuscript and approving it for publication was Ángel F. García-Fernández.

and advance diverse zeroing neural network (ZNN) models for addressing time-varying challenges [15], [16], [17], [18], [19]. These encompass a range of scenarios, including time-varying linear equations [16], [19], time-variant Sylvester equations [17], Stein matrix inversion [18], non-convex optimization [15], among others. The time-varying matrix inversion problem validated in this paper constitutes one such instance of these time-varying challenges.

The assessment of the ZNN model's superior performance primarily focuses on two key indicators: convergence performance and noise tolerance. Convergence performance is typically enhanced by optimizing the ZNN models' convergence behavior using various types of activation functions, including linear activation functions (LAF), versatile activation functions [20], and novel activation functions [21]. Additionally, accelerating convergence speed and precision can be achieved by introducing varying parameters and variable gain. For instance, in the study [19], [22], a variable gain $g(t, x)$ is employed, while Tan et al. in [23] utilize $\Gamma(t) = (t^{\mathrm{p}} + \mathrm{p})$.

Another aspect is the tolerance to noise, in practical application domains, various types of noise persist and are unavoidable, including constant static noise, time-dependent linear noise, time-dependent harmonic noise, and so forth. The OZNN can only handle TVMI under ideal no noise conditions. Therefore, some ZNN models [21], [24], [25], [26], [27], [28]have been proposed to address time-varying problems under additional noise interference. For harmonic noise, Guo et al. proposed the modified ZNN specifically to suppress harmonic noise [25]. By adding an adaptation term for harmonic noise to the OZNN model, the ZNN model's noise suppression capability is enhanced. Inspired by PID control theory [29], Jin et al. introduced a single integral term into the model, proposing a noise-tolerant ZNN model capable of tolerating various types of noise [26], [27], [28]. Building upon this design, Xiao et al. incorporated a novel activation function (NAF) and devised the NNTZNN model [21].

However, single-noise-tolerant ZNN models have limited tolerance to certain types of noise [21], [30], and their convergence speed is relatively slow. To address this challenge, in the field of time-varying matrices, this paper introduces the dual noise tolerant ZNN (DNTZNN) model by leveraging the accelerating and noise reducing properties of double integration, enhancing the ZNN model's tolerance to various noises (e.g., constant noise, time dependent unbounded noise (linear noise), time dependent bounded noise (harmonic noise)).

In the field of artificial intelligence, activation functions hold significant importance. As mentioned earlier, in the ZNN domain, as discussed above, activation functions typically accelerate convergence and suppress noise. Inspired by numerous studies [17], [31], [32], [33], [34], [35], [36] utilizing activation functions,this paper introduces a positive odd activation function into the framework of the DNTZNN model, resulting in the development of the triple noise-tolerant ZNN (TNTZNN) model. This ZNN model further enhances its tolerance to noise.

The principal academic contributions of this paper are outlined as follows: Firstly, to address TVMI problems under various noise disturbances, we introduced the DNTZNN model, leveraging the acceleration and noise reduction capabilities of dual integration. Building on this, we designed the TNTZNN model by integrating a positive odd activation function, resulting in faster convergence and stronger noise tolerance. Secondly, we conducted a convergence analysis and robustness analysis against various noises for the TNTZNN model based on the Lyapunov theorem. The theoretical proof demonstrates that the TNTZNN model has superior noise tolerance compared to the IEZNN model, with an inherent structural advantage. Furthermore, quantitative comparative experiments with two different types of time-varying matrices validated the efficient convergence and superiority of the TNTZNN model in noise-free conditions. Three sets of noise comparison experiments confirmed the model's strong noise tolerance. Experiments with high-dimensional complex matrices demonstrated the model's robust noise tolerance and convergence performance for higher-dimensional and more complex matrices. To the best of the authors' understanding, no ZNN model offering triple noise tolerance for time-varying matrix inversion has been put forth thus far.

The paper is structured into six sections. The second section delves into the problem of TVMI and introduces the related ZNN and IEZNN models. In the third section, the DNTZNN model is introduced, and the activation function is chosen via a lemma, followed by the design of the TNTZNN model. In the fourth section, the Lyapunov theorem is applied to theoretically demonstrate the convergence and resilience of the TNTZNN model against noise, alongside an analysis of its inherent structural advantages over the IEZNN model in terms of noise tolerance. The fifth section presents comprehensive comparative experiments, illustrating the superior convergence performance and noise resilience of the TNTZNN model, as well as its ability to generalize in high-dimensional complex matrices. Finally, the sixth section offers a succinct summary of the paper.

II. PROBLEM FORMULATIONS AND RELATED MODELS

The problem of time-varying matrix inversion and the related solution models will be presented in this section.

A. CONSIDERATION OF THE TVMI PROBLEM

The TVMI problem can be described as follows:

$$A(t)B(t) = I, \quad \text{or} \quad B(t)A(t) = I \in \mathbb{R}^{n\times n}, \tag{1}$$

in which $A(t) \in \mathbb{R}^{n\times n}$ is a non-singular smooth coefficient matrix varying with time, with rank n, and $B(t) \in \mathbb{R}^{n\times n}$, an unknown matrix which is the inverse of A(t), and I as the identity matrix. Based on the DNTZNN model and TNTZNN model, the goal of this paper is to rapidly and accurately solve

for the inverse $B(t)$ of the matrix $A(t)$ under various noise interferences.

B. OZNN AND IEZNN MODEL

As discussed in [26], OZNN represents a dynamic method grounded in error functions, ensuring the error function converges to zero. Under noise-free circumstances, a matrix-form error function is delineated to oversee the resolution of the TVMI problem.

Its formula is devised as follows:

$$E(t) = A(t)B(t) - I. \tag{2}$$

Derivation of (2) yields

$$\dot{E}(t) = \dot{A}(t)B(t) + A(t)\dot{B}(t). \tag{3}$$

The design formula for the OZNN model is as follows:

$$\dot{E}(t) = -hE(t), \tag{4}$$

in which, h is the design parameter, $h > 0 \in \mathbb{R}$ used to accelerate the convergence rate. We introduce noise into Equation (4) as follows:

$$\dot{E}(t) = -hE(t) + N(t), \tag{5}$$

where $N(t) \in \mathbb{R}^{n\times n}$ is the matrix-form noise. By combining (3) and (5), we obtain the following equation:

$$A(t)\dot{B}(t) = -\dot{A}(t)B(t) - h(A(t)B(t) - I) + N(t). \tag{6}$$

In reality, various types of noise exist, including constant noise, environmental noise, interference noise, and so forth. However, the OZNN model cannot effectively suppress these noises. Therefore, inspired by PID control theory, the IEZNN model is proposed to overcome this issue. Its design formula is expressed as follows:

$$\dot{E}(t) = -hE(t) - \lambda\int_0^t E(\tau)\mathrm{d}\tau + N(t), \tag{7}$$

where $h, \lambda > 0$ are design parameters used to adjust the convergence rate. It's worth noting that the integral term is used to eliminate error. The detailed IEZNN model under noise interference is expressed as follows:

$$\begin{aligned} A(t)\dot{B}(t) = &-\dot{A}(t)B(t) - h(A(t)B(t) - I) \\ &- \lambda\int_0^t (A(\tau)B(\tau) - I)\mathrm{d}\tau + N(t) \end{aligned} \tag{8}$$

As shown in [26], through theoretical analysis and comparative experiments, it is demonstrated that IEZNN can better handle TVMI problems under various noise interferences.

III. TNTZNN MODEL

Although IEZNN can partially suppress noise, it requires further refinement as it can only converge its error function to zero in TVMI problems under constant noise environments. However, it fails to fully tolerate unbounded linear noise and bounded random noise (e.g., harmonic noise). To tackle this limitation, the DNTZNN model is developed, leveraging the robust acceleration and noise reduction capabilities of double integration.

A. DNTZNN MODEL INTRODUCED

The error function equation for DNTZNN under noise interference is as follows:

$$\begin{aligned} \dot{E}(t) = &-(2\xi + h)E(t) - (2\xi h + \xi^2)\int_0^t E(\tau)\mathrm{d}\tau \\ &- \xi^2 h\int_0^t\int_0^\tau E(\sigma)\mathrm{d}\sigma\mathrm{d}\tau + N(t), \end{aligned} \tag{9}$$

where $\xi, h > 0$ are design parameters. We substitute $E(t) = A(t)B(t) - I$ and the detailed dual noise tolerant zeroing neural network model can be obtained as:

$$\begin{aligned} A(t)\dot{B}(t) = &-\dot{A}(t)B(t) - (2\xi + h)(A(t)B(t) - I) \\ &- (2\xi h + \xi^2)\int_0^t (A(\tau)B(\tau) - I\mathrm{d}\tau \\ &- \xi^2 h\int_0^t\int_0^\tau (A(\sigma)B(\sigma) - I\mathrm{d}\sigma\mathrm{d}\tau \\ &+ N(t). \end{aligned} \tag{10}$$

B. TNTZNN MODEL DESIGN

In the domain of neural networks, activation functions hold significant importance. Within the realm of zeroing neural networks, activation functions typically demonstrate noise reduction and acceleration of convergence effects. Building upon this notion, we introduce positive odd activation functions into the framework of the DNTZNN model. Common types of positive odd activation functions encompass linear-like, sigmoid-like, signal-like, composite trigonometric functions, among others [[17], [19], [22]]. In this study, we exemplify with the Power Activation Function (PAF), Power Sigmoid Activation Function (PSAF), and Signal-Bi-Power Activation Function (SBPAF). The explicit forms of these positive odd activation functions are delineated below:

- PAF:

$$\Phi_1(x) = x^3 \tag{11}$$

- PSAF:

$$\Phi_2(x) = \begin{cases} x^{r_1}, & \text{if} |x| \geq 1 \\ \dfrac{1+\exp(-r_2)}{1-\exp(-r_2)} \cdot \dfrac{1-\exp(-r_2 x)}{1+\exp(-r_2 x)}, & \text{if} |x| < 1 \end{cases} \tag{12}$$

  where,$r_1 \geq 0$, p is odd,$r_2 \geq 3$.

- SBPAF:

$$\Phi_3(x) = (k_1|x|^\eta + k_2|x|^\omega)sign(x) + k_3 x, \tag{13}$$

  where $sign(\cdot)$ is a symbolic function,and design parameters are $k_1 > 0, k_2 > 0, k_3 > 0, \eta > 0, 0 < \omega < 1$.

However, finding the most suitable activation function is a challenging task. Zhang et al. [22], based on the Lyapunov stability framework, proposed a convergence time theorem, which indicates that the convergence speed of a system is correlated with the derivative near its origin. Specifically, the larger the absolute value of the derivative, the shorter

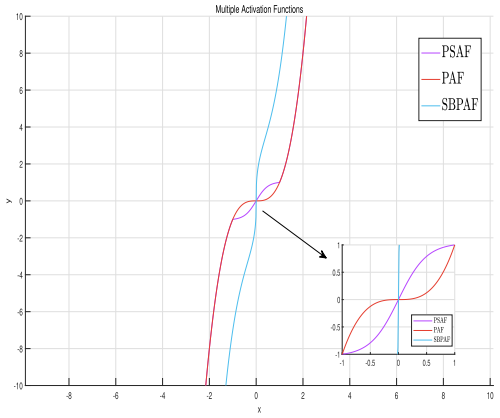

FIGURE 1. Three sorts of positive odd activation functions are presented: Power Activation Function (PAF) (red solid line), Power Sigmoid Activation Function (PSAF) (purple solid line, $r_1 = 3, r_2 = 4$), Signal Bi-Power Activation Function (SBPAF) (blue solid line, $k_1 = 2, k_2 = 4, k_3 = 1, \eta = 3, \omega = \frac{1}{3}$).

the convergence time of the system, and the more stable the model. According to the above theorem and Figure 1, it can be concluded that SBPAF outperforms PSAF, and PSAF outperforms PAF. Therefore, SBPAF, as a positive odd function, is used in this paper.

Therefore OZNN adopts the following design equation:

$$\dot{E}(t) = -h\Phi(E(t)) \tag{14}$$

in which, $\Phi(\cdot)$: $\mathbb{R}^{n\times n} \to \mathbb{R}^{n\times n}$ is an array of positive odd activation functions.

Shifting the right side of the equation to the left side of the equation, we get

$$\dot{E}(t) + h\Phi(E(t)) = 0.$$

We let

$$S(t) = \dot{E}(t) + h\Phi(E(t)), \tag{15}$$

and set

$$S(t) = -\xi \int_0^t S(\tau)\mathrm{d}\tau. \tag{16}$$

Combining (15) and (16), we get

$$\dot{E}(t) = -h\Phi(E(t)) - \xi \int_0^t S(\tau)\mathrm{d}\tau \tag{17}$$

and

$$\begin{aligned}\dot{E}(t) + h\Phi(E(t)) &= -\xi \int_0^t S(\tau)\mathrm{d}\tau \\ &= -\xi \int_0^t (\dot{E}(\tau) + h\Phi(E(\tau)))\mathrm{d}\tau \\ &= -\xi E(t) - \xi h \int_0^t (E(t))\mathrm{d}\tau. \end{aligned} \tag{18}$$

Similarly, we let

$$L(t) = \dot{E}(t) + \xi E(t) + h\Phi(E(t)) + \xi h \int_0^t \Phi(E(\tau))\mathrm{d}\tau, \tag{19}$$

setting,

$$L(t) = \xi \int_0^t (L(t))\mathrm{d}\tau. \tag{20}$$

Bringing (19) into (20) yields

$$\begin{aligned}&\dot{E}(t) + \xi E(t) + h\Phi(E(t)) + \xi h \int_0^t (\Phi(E(\tau)))\mathrm{d}\tau \\ &= -\xi \int_0^t (\dot{E}(\tau) + \xi E(\tau) + h\Phi(E(\tau)) \\ &\quad + \xi h \int_0^\tau (\Phi(E(\delta)))\mathrm{d}\delta)\mathrm{d}\tau \\ &= -\xi E(t) - \xi^2 \int_0^t E(\tau)\tau - \xi h \int_0^t \Phi(E(\tau))\mathrm{d}\tau \\ &\quad - \xi^2 h \int_0^t \int_0^\tau \Phi(E(\delta))\mathrm{d}\delta\mathrm{d}\tau. \end{aligned} \tag{21}$$

Rearranging (21), we get the following TNTZNN model as follows:

$$\begin{aligned}\dot{E}(t) = &-\xi^2 h \int_0^t \int_0^\tau \Phi(E(\delta))\mathrm{d}\delta\mathrm{d}\tau \\ &- 2\xi h \int_0^t \Phi(E(\tau))\mathrm{d}\tau \\ &- \xi^2 \int_0^t (E(\tau))\mathrm{d}\tau \\ &- 2\xi E(t) - h\Phi(E(t)). \end{aligned} \tag{22}$$

Adding the effect of noise, the TNTZNN model is rewritten as the following equation:

$$\begin{aligned}\dot{E}(t) = &-\xi^2 h \int_0^t \int_0^\tau \Phi(E(\delta))\mathrm{d}\delta\mathrm{d}\tau \\ &- 2\xi h \int_0^t \Phi(E(\tau))\tau \\ &- \xi^2 \int_0^t (E(\tau))\mathrm{d}\tau \\ &- 2\xi E(t) - h\Phi(E(t)) + N(t). \end{aligned} \tag{23}$$

Bringing (2) and (3) into the above equation, the detailed TNTZNN model is obtained as follows:

$$\begin{aligned}A(t)\dot{B}(t) = &-\dot{A}(t)B(t) - \xi^2 h \int_0^t \Phi(A(\delta)B(\delta) - I)\mathrm{d}\delta\mathrm{d}\tau \\ &- 2\xi h \int_0^t \Phi(A(\tau)B(\tau) - I)\mathrm{d}\tau \\ &- \xi^2 \int_0^t (A(\tau)B(\tau) - I)\mathrm{d}\tau \\ &- 2\xi(A(t)B(t) - I) \\ &-h\Phi(A(t)B(t) - I) + N(t) \end{aligned} \tag{24}$$

Bringing the specific positive odd activation function SBPAF $\Phi(x) = (2|x|^3 + 4|x|^{1/3})sign(x) + x$, chosen above brought into (24) is obtained

$$\begin{aligned}A(t)\dot{B}(t) = &-\dot{A}(t)B(t) - \xi^2 h \int_0^t \int_0^\tau (2|A(\delta)B(\delta) - I|^3 \\ &+ 4|A(\delta)B(\delta) - I|^{1/3} sign(A(\delta)B(\delta) - I)\end{aligned}$$

$$
\begin{aligned}
&+ (A(\delta)B(\delta) - I))\mathrm{d}\delta\mathrm{d}\tau \\
&- 2\xi h \int_0^t (2|A(\delta)B(\delta) - I|^3 \\
&+ 4|A(\delta)B(\delta) - I|^{1/3} sign(A(\delta)B(\delta) - I) \\
&+ (A(\delta)B(\delta) - I))\mathrm{d}\delta \\
&- \xi^2 \int_0^t (A(\tau)B(\tau) - I)\mathrm{d}\tau - 2\xi(A(t)B(t) - I) \\
&-h(2|A(t)B(t) - I|^3 \\
&+ 4|A(t)B(t) - I|^{1/3} sign(A(t)B(t) - I) \\
&+ (A(t)B(t) - I)) + N(t)
\end{aligned} \tag{25}
$$

IV. THEORETICAL ANALYSES

A. CONVERGENCE

Theorem 1: For a non-singular, smooth time-varying matrix $A(t) \in \mathbb{R}^{n\times n}$, the TNTZNN model, equipped with a positive odd activation function $\Phi(\cdot)$, achieves convergence towards the theoretical inverse of the time-varying matrix $A(t)$. This convergence initiates from an arbitrary initial value $B(0) \in \mathbb{R}^{n\times n}$ and proceeds towards the theoretical inverse $A^{-1}(t) \in \mathbb{R}^{n\times n}$ as $t \to \infty$. In essence, as $t \to \infty$, the Frobenius norm of the error matrix $\mathbf{E}(t)$ tends towards zero:

$$\lim_{t\to\infty} \|\mathbf{E}(t)\|_F = 0$$

The proof of Theorem 1 proceeds as follows.

Proof: From the previous subsection, we have

$$\begin{cases} L(t) = -\xi \int_0^t L(\tau)\mathrm{d}\tau, \\ \dot{L}(t) = -\xi L(t), \end{cases} \quad \xi > 0, \tag{26}$$

and their elemental terms are

$$\begin{cases} l_{ij}(t) = -\xi \int_0^t l_{ij}(\tau)\mathrm{d}\tau, \\ \dot{l}_{ij}(t) = -\xi l_{ij}(t), \end{cases} \tag{27}$$

A Lyapunov function is defined as follows:

$$\epsilon(t) = l_{ij}^2(t). \tag{28}$$

Its derivative is

$$\dot{\epsilon}(t) = 2\dot{l}_{ij}(t)l_{ij}(t). \tag{29}$$

Combining (27) and (29), we obtain

$$\dot{\epsilon}(t) = -\xi l_{ij}^2(t). \tag{30}$$

As $t \to \infty$, it is evident that $\epsilon(t)$ is positive definite, and its derivative $\dot{\epsilon}(t)$ is negative definite. According to Lyapunov stability theory, we deduce that

$$\lim_{t\to\infty} |\epsilon(t)| = \lim_{t\to\infty} |l_{ij}^2(t)| = \lim_{t\to\infty} |l_{ij}(t)| = 0. \tag{31}$$

The sub-elements of (19) can be expressed as

$$l_{ij}(t) = \dot{e}_{ij}(t) + \xi e_{ij}(t) + h\Phi(e_{ij}(t)) + \xi h \int_0^t \Phi(e_{ij}(\tau))\mathrm{d}\tau, \tag{32}$$

and the sub-elements of (15) can be expressed as

$$s_{ij}(t) = \dot{e}_{ij}(t) + h\Phi(e_{ij}(t)), \tag{33}$$

where $e_{ij}(t)$ and $s_{ij}(t)$ are the element terms of row i and column j of $E(t)$ and $S(t)$ respectively. By combining (32) and (33), we obtain

$$l_{ij}(t) = s_{ij}(t) + \xi \int_0^t s_{ij}(\tau)\mathrm{d}\tau. \tag{34}$$

Then, from (34), we can deduce

$$\lim_{t\to\infty} |l_{ij}(t)| = \lim_{t\to\infty} |s_{ij}(t) + \xi \int_0^t s_{ij}(\tau)\mathrm{d}\tau| = 0. \tag{35}$$

From (35), we obtain

$$\begin{cases} s_{ij}(t) = -\xi \int_0^t s_{ij}(\tau)\mathrm{d}\tau, \\ \dot{s}_{ij}(t) = -\xi s_{ij}(t), \end{cases} \quad \text{as} \quad t \to \infty, \tag{36}$$

and we design another Lyapunov function as follows:

$$\rho(t) = s_{ij}^2(t). \tag{37}$$

Deriving the above equation, we get

$$\dot{\rho}(t) = 2\dot{s}_{ij}(t)s_{ij}(t) = -2\xi s_{ij}^2(t) < 0. \tag{38}$$

Similarly, since $\rho(t) \geq 0$, $\dot{\rho}(t) \leq 0$, $\rho(t)$ is globally asymptotically stable. We can deduce:

$$\lim_{t\to\infty} |s_{ij}(t)| = 0.$$

Due to $s_{ij}(t) = e_{ij}(t) + h\Phi(e_{ij}(t))$,

$$\lim_{t\to\infty} |\dot{e}_{ij}(t) + h\Phi(e_{ij}(t))| = 0, \tag{39}$$

then, we obtain $\dot{e}_{ij} = -h\Phi(e_{ij}(t))$, as $t \to \infty$.

By the same method, we define a Lyapunov function

$$\eta(t) = e_{ij}^2(t). \tag{40}$$

We obtain that

$$\dot{\eta}(t) = 2\dot{e}_{ij}(t)e_{ij}(t) = -2h\Phi(e_{ij}(t))e_{ij}(t). \tag{41}$$

Since $\Phi(.)$ is a positive odd function and does not change sign, we have

$$\dot{\eta}(t) \leq 0.$$

Therefore, we conclude that $\eta(t)$ is globally asymptotically stable, so that

$$\lim_{t\to\infty} |\eta(t)| = \lim_{t\to\infty} |e_{ij}^2(t)| = \lim_{t\to\infty} |e_{ij}(t)| = 0. \tag{42}$$

Thus (42) is converted to matrix form as

$$\lim_{t\to\infty} \|\mathbf{E}(t)\|_F = 0. \tag{43}$$

Thus, Theorem 1 is proven. ■

B. ROBUSTNESS TO NOISE

In various practical industrial application scenarios, noise exists and is unavoidable, so it is necessary to take noise into consideration. In this subsection, we mainly discuss and analyse the robustness of TNTZNN under noise interference.

Theorem 2: For a non-singular, smooth time-varying matrix $A(t) \in \mathbb{R}^{n\times n}$, along with the identity matrix $I \in \mathbb{R}^{n\times n}$, and considering any initial value $B(0)$, the TNTZNN model, incorporating a positive odd activation function $\Phi(\cdot)$, swiftly converges to its theoretical solution $A^{-1}(t) \in \mathbb{R}^{n\times n}$, despite the presence of a constant but unknown noise $N(t) \in \mathbb{R}^{n\times n}$. This convergence is characterized by the Frobenius norm of the error matrix $\mathbf{E}(t)$ approaching zero as $t \to \infty$,

$$\lim_{t\to\infty} \|\mathbf{E}(t)\|_F = 0$$

Proof: The proof of Theorem 2 is as follows. The constant noise can be expressed in the following form

$$N(t) = P, \tag{44}$$

where P is a constant coefficient matrix belonging to $\mathbb{R}^{n\times n}$. Its elemental terms are written as:

$$n_{ij}(t) = p_{ij}. \tag{45}$$

When there is constant noise interference, (20) can be transformed into

$$L(t) = -\xi \int_0^t (L(\tau))\mathrm{d}\tau + N(t), \tag{46}$$

and the corresponding elemental terms are

$$l_{ij}(t) = -\xi \int_0^t (l_{ij}(\tau))\mathrm{d}\tau + n_{ij}(t). \tag{47}$$

Incorporating $n_{ij}(t)$, we get

$$l_{ij}(t) = -\xi \int_0^t (l_{ij}(\tau))\mathrm{d}\tau + p_{ij}. \tag{48}$$

Taking the first and second derivatives of the above equation, we get

$$\begin{cases} \dot{l}_{ij}(t) = -\xi l_{ij}(t), \\ \ddot{l}_{ij}(t) = -\xi \dot{l}_{ij}(t). \end{cases} \tag{49}$$

Suppose a Lyapunov function

$$\theta(t) = l_{ij}^2(t). \tag{50}$$

Deriving it yields

$$\dot{\theta}(t) = 2\dot{l}_{ij}(t)l_{ij}(t) = -2\xi l_{ij}^2(t). \tag{51}$$

Since $\theta \geq 0$ and $\dot{\theta} \leq 0$, signifying the Lyapunov stability condition, $\theta(t)$ is globally asymptotically stable, and hence we get

$$\lim_{t\to\infty} |\theta(t)| = \lim_{t\to\infty} |l_{ij}^2(t)| = \lim_{t\to\infty} |l_{ij}(t)| = 0. \tag{52}$$

Since

$$l_{ij}(t) = s_{ij}(t) + \xi \int_0^t s_{ij}(\tau)\mathrm{d}\tau,$$

so,

$$\lim_{t\to\infty} |s_{ij}(t) + \xi \int_0^t s_{ij}(\tau)\mathrm{d}\tau| = 0. \tag{53}$$

Derivation of this yields

$$\lim_{t\to\infty} |\dot{s}_{ij}(t) + \xi s_{ij}(t)| = 0, \tag{54}$$

and

$$\dot{s}_{ij}(t) = -\xi s_{ij}(t), \quad t \to \infty.$$

This equation is the same as (36) in Theorem 1, so it is easy to derive

$$\lim_{t\to\infty} |e_{ij}(t)| = 0,$$

and the corresponding matrix form

$$\lim_{t\to\infty} \|\mathbf{E}(t)\|_F = 0.$$

The proof is complete. ■

Theorem 3: For a non-singular, smooth time-varying matrix $A(t) \in \mathbb{R}^{n\times n}$ and its corresponding unit matrix $I \in \mathbb{R}^{n\times n}$, the TNTZNN model, incorporating a positive singular activation function $\Phi(\cdot)$, demonstrates rapid convergence to the theoretical solution $A^{-1}(t) \in \mathbb{R}^{n\times n}$ in the presence of linear noise in matrix form, starting from any initial value $B(0)$. Put differently,

$$\lim_{t\to\infty} \|\mathbf{E}(t)\|_F = 0.$$

Proof: The proof of Theorem 3 is as follows. The linear noise can be expressed as follows:

$$N(t) = Pt + Q \in \mathbb{R}^{n\times n}, \tag{55}$$

where $P \in \mathbb{R}^{n\times n}$ and $Q \in \mathbb{R}^{n\times n}$ are constant coefficient matrices, and their elemental terms are written as

$$n_{ij}(t) = p_{ij}t + q_{ij}. \tag{56}$$

According to equations (26) and (27) in Theorem 1, the TNTZNN model under linear noise interference can be written as

$$L(t) = -\xi \int_0^t (L(\tau))\mathrm{d}\tau + N(t), \tag{57}$$

and its sub-element terms are

$$l_{ij}(t) = -\xi \int_0^t (l_{ij}(\tau))\mathrm{d}\tau + n_{ij}(t). \tag{58}$$

Taking the derivative of $l_{ij}(t)$ once, we get

$$\dot{l}_{ij}(t) = -\xi l_{ij}(t) + n_{ij}(t). \tag{59}$$

Taking the second derivative, we get

$$\ddot{l}_{ij}(t) = -\xi \dot{l}_{ij}(t) + \dot{n}_{ij}(t) \tag{60}$$

Differentiating linear noise separately, we have

$$\begin{cases} \dot{n}_{ij}(t) = p_{ij} \\ \ddot{n}_{ij}(t) = 0. \end{cases}$$

Hence, $\ddot{l}_{ij}(t) = -\xi \dot{l}_{ij}(t)$.

We define a Lyapunov function as

$$\vartheta(t) = \dot{l}_{ij}^2(t). \tag{61}$$

Thus,

$$\dot{\vartheta}(t) = 2\ddot{l}_{ij}(t)\dot{l}_{ij}(t) = -\xi \dot{l}_{ij}^2(t). \tag{62}$$

Since $\vartheta \geq 0$ is positive definite, and its derivative $\dot{\vartheta} \leq 0$ is negative definite, therefore, $\vartheta(t)$ is globally asymptotically stable and, we get

$$\lim_{t\to\infty} |\vartheta(t)| = \lim_{t\to\infty} |l_{ij}^2(t)| = \lim_{t\to\infty} |l_{ij}(t)| = 0. \tag{63}$$

Substituting (59) back in, we get

$$\lim_{t\to\infty} |\dot{l}_{ij}(t)| = \lim_{t\to\infty} | - \xi l_{ij}(t) + \dot{n}_{ij}(t)| = 0. \tag{64}$$

Using $\dot{n}_{ij}(t) = p_{ij}$, we have

$$\lim_{t\to\infty} | - \xi l_{ij}(t) + p_{ij}| = 0.$$

Thus, we conclude

$$\lim_{t\to\infty} |l_{ij}(t)| = \frac{p_{ij}}{\xi}.$$

Taking the derivative, we get

$$\lim_{t\to\infty} |\dot{s}_{ij}(t) + \xi s_{ij}(t)| = 0, \tag{65}$$

which implies

$$\dot{s}_{ij}(t) = -\xi s_{ij}(t), \quad t \to \infty.$$

Notice that the above equation is the same as (36), so it is easy to deduce that

$$\lim_{t\to\infty} |e_{ij}(t)| = 0,$$

and the corresponding matrix form

$$\lim_{t\to\infty} \|\mathbf{E}(t)\|_F = 0.$$

Thus, Theorem 3 is proven. ■

It's noteworthy that since $\Phi_3(x)$ represents a specific form of the positive odd function $\Phi(x)$, the TNTZNN model employing $\Phi_3(x)$ SBPAF (25) also satisfies the convergence and robustness theories mentioned above. The methodology for establishing the convergence and robustness of the DNTZNN model closely mirrors that of the TNTZNN, thus necessitating no extensive elaboration here.

It is also worth noting that Jin et al. in their paper [26] mentioned that when the IEZNN is contaminated by matrix-form linear noise, its steady-state error is given by

$$\lim_{t\to\infty} \|E(t)\|_F = \frac{\|N(t)\|_F}{\xi}$$

where $\xi > 0$. In contrast, the TNTZNN model proposed in this paper, under linear noise interference, exhibits a limit of the steady-state error approaching 0. This theoretically demonstrates the inherent superiority of the double integration structure in the TNTZNN model for noise suppression.

V. SIMULATION AND COMPARATIVE NUMERICAL EXPERIMENTS

In this section, three sets of comparative numerical experiments are conducted to validate the effectiveness and superiority of the TNTZNN model over the DNTZNN model and IEZNN model in handling time-varying problems, as well as its tolerance to various types of noise and its generalization capability to high-dimensional matrices. For the sake of comparison and simplicity, all design parameters of the three models are set to 4.

Convergence serves as a pivotal indicator for evaluating the efficacy of ZNN models. In this experiment, we conduct a comparative analysis of the convergence time among the IEZNN, DNTZNN, and TNTZNN models to delineate their convergence characteristics. The convergence and efficacy of the TNTZNN model in tackling the TVMI problem are validated through two sets of model comparison experiments with fixed initial values.

A. EXPERIMENT 1: CONVERGENCE

A two-dimensional time-varying matrix is delineated as follows:

$$A(t) = \begin{bmatrix} \sin(3t) & \cos(3t) \\ -3\cos(3t) & 3\sin(3t) \end{bmatrix} \in \mathbb{R}^{2\times 2}. \tag{66}$$

To demonstrate the efficacy of the TNTZNN model in solving the TVMI problem, we numerically compute the theoretical inverse of the aforementioned time-varying matrix as follows:

$$A^{-1}(t) = \begin{bmatrix} \sin(3t) & -1/3\cos(3t) \\ \cos(3t) & 1/3\sin(3t) \end{bmatrix} \in \mathbb{R}^{2\times 2}. \tag{67}$$

In the absence of noise, we compared the IEZNN, DNTZNN, and TNTZNN models with their design parameters set to 4. They all started from the same initial state

$$B(0) = \begin{bmatrix} 3 & 3 \\ 3 & 3 \end{bmatrix}.$$

The corresponding findings are depicted in Fig. 2(a) and Fig. 2(b). From the trajectory plot of neural states in Fig. 2(a), it is apparent that the solution state $B(t)$ derived by the IEZNN model converges to the theoretical solution $A(t)^{-1}$ within 3.7 seconds, whereas the DNTZNN model achieves proximity to the theoretical inverse $A(t)^{-1}$ within 2.3 seconds. In contrast, the TNTZNN model achieves convergence to the theoretical solution within a mere 0.3 seconds, outperforming the IEZNN model by a factor of 12 and the DNTZNN model by a factor of 7 in terms of speed. This underscores the efficiency and superior convergence capability of the TNTZNN model in addressing the TVMI problem.

To further substantiate the convergence, efficacy, and superiority of the TNTZNN model, we propose an additional set of matrices as follows:

$$A(t) = \begin{bmatrix} \exp(3t) & -\exp(3t)+1 \\ -\exp(3t)+1 & \exp(3t) \end{bmatrix} \in \mathbb{R}^{2\times 2}. \tag{68}$$

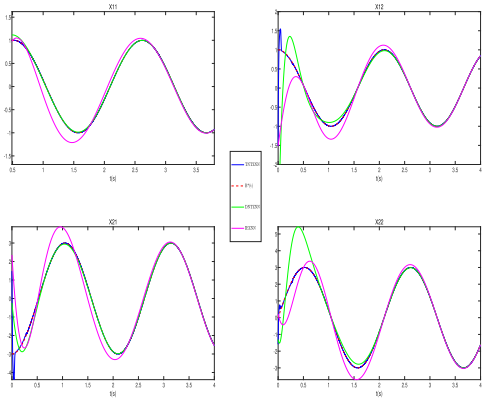

(a) Trajectory of TNTZNN model (25)(blue solid line), DNTZNN model (10) (green solid line) and the IEZNN model (8) (pink solid line) for solving the TVMI problem (66), in which the red dashed-dotted curves align with to the theoretical inverse B*(t).

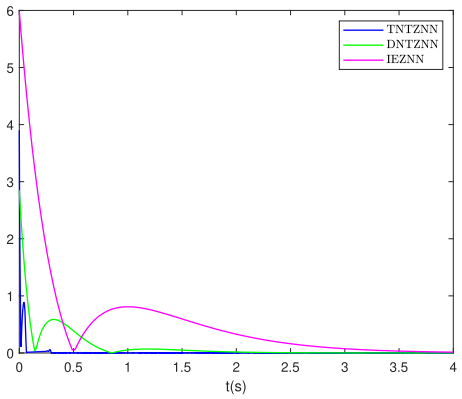

(b) Residual errors of the TNTZNN model (25)(blue solid line) , DNTZNN model (10) (green solid line) and IEZNN model (8) (pink solid line) with the same initial state B(0) for solving the TVMI problem (66) under no noise.

FIGURE 2. Convergence comparision of IEZNN, DNTZNN and TNTZNN.

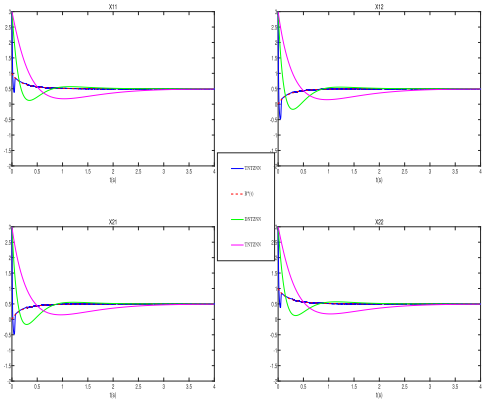

(a) Trajectory of TNTZNN model (25)(blue solid line), DNTZNN model (10) (green solid line) and the IEZNN model (8) (pink solid line) for solving the TVMI problem (68), in which the red dashed-dotted curves align with to the theoretical inverse B*(t).

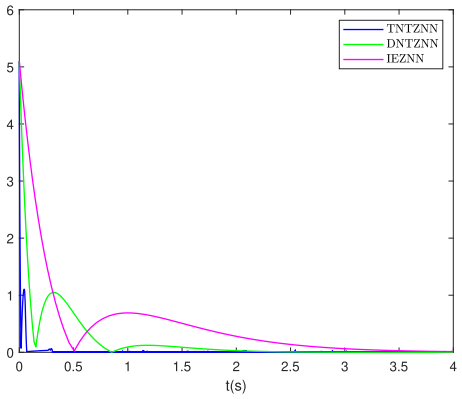

(b) Residual errors of the TNTZNN model (25)(blue solid line) , DNTZNN model (10) (green solid line) and IEZNN model (8) (pink solid line) with the same initial state B(0) for solving the TVMI problem (68) under no noise.

FIGURE 3. Convergence comparision of IEZNN, DNTZNN and TNTZNN.

Its theoretical inverse is represented as shown below:

$$A^{-1}(t) = \frac{1}{2\exp(3t) - 1}\begin{bmatrix} \exp(3t) & 1-\exp(3t) \\ 1-\exp(3t) & \exp(3t) \end{bmatrix} \in \mathbb{R}^{2\times 2}. \tag{69}$$

The initial conditions and design parameters of the IEZNN, DNTZNN, and TNTZNN models remain consistent. Their neural state trajectory plots and residual error plots are depicted in Fig. 3(a) and 3(b), respectively. From Fig. 3(b), it is evident that the residual errors $\|E(t)\|_F = \|A(t)B(t) - I\|_F$ of the IEZNN model converge to 0 within 3.8 seconds, the DNTZNN model within 2.3 seconds, and the TNTZNN model within 0.3 seconds. This observation suggests that even when applied to more generalized time-varying matrices, these three models demonstrate similar convergence behaviors, further affirming the efficacy and superiority of the TNTZNN model.

In the subsequent experiment, a comparative analysis of the three models will be undertaken under diverse matrix noise conditions to further corroborate the convergence and tolerance capabilities of the TNTZNN model.

B. EXPERIMENT 2: ROBUSTNESS TO VARIOUS NOISES

In this experimental set, we compared the tolerance capabilities of the IEZNN, DNTZNN, and TNTZNN models to various forms of noise. For simplicity, all design parameters of these three models were set to 4. We conducted experiments using the time-varying matrix (66) from Experiment 1.

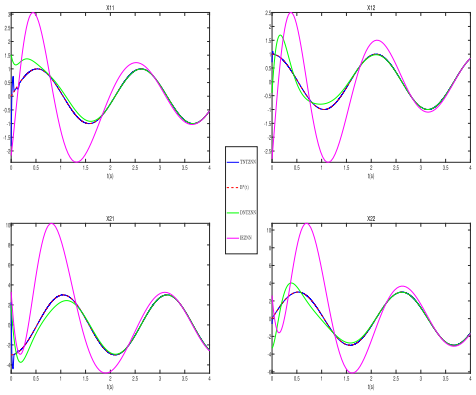

(a) Trajectory of TNTZNN model (25)(blue solid line), DNTZNN model (10) (green solid line) and the IEZNN model (8) (pink solid line) for solving the TVMI problem (66) under constant noise, in which the red dashed-dotted curves align with to the theoretical inverse B*(t).

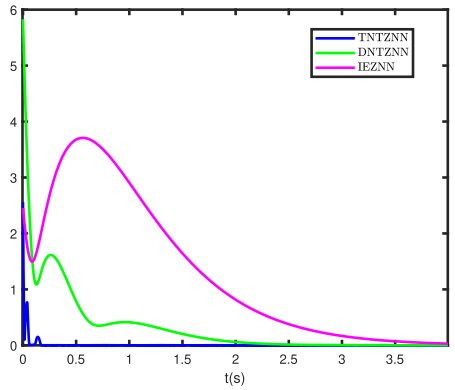

(b) Residual errors of the TNTZNN model (25)(blue solid line) , DNTZNN model (10) (green solid line) and IEZNN model (8) (pink solid line) with any initial state B(0) for solving the TVMI problem (66) under constant noise.

FIGURE 4. Robustness comparision of IEZNN, DNTZNN and TNTZNN.

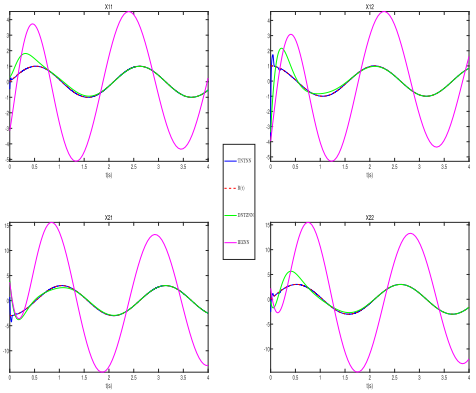

(a) Trajectory of TNTZNN model (25) (blue solid line), DNTZNN model (10) (green solid line), and IEZNN model (8) (pink solid line) for solving the TVMI problem (66) under linear noise. The red dashed-dotted curves align with the theoretical inverse $B^*(t)$.

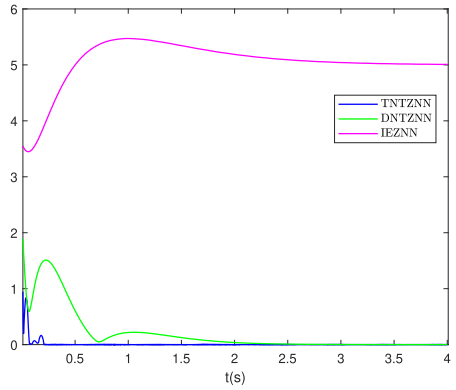

(b) Residual errors of the TNTZNN model (25) (blue solid line), DNTZNN model (10) (green solid line), and IEZNN model (8) (pink solid line) with any initial state $B(0)$ for solving the TVMI problem (66) under linear noise.

FIGURE 5. Robustness comparison of IEZNN, DNTZNN, and TNTZNN.

We considered the following three types of noise scenarios for computer simulations of TVMI:

1) Constant noise
2) Linear time-varying noise
3) Bounded noise(such as harmonic noise)

Now, we begin to investigate the case of constant noise.

1) CONSTANT NOISE

In numerous hardware implementations, constant noise is an inherent challenge. For the sake of comparison, every element of the constant noise matrix is set to 10. The comparative residual error outcomes of the IEZNN, DNTZNN, and TNTZNN models for addressing the TVMI issue amid constant noise, commencing from any initial value $B(0) \in [-4, 4]^{2\times 2}$, are depicted in Fig. 4(b).

From the observations derived from Fig. 4(b), it's apparent that IEZNN, DNTZNN, and TNTZNN all display some level of noise mitigation in the presence of constant noise. Nonetheless, IEZNN achieves error convergence to zero approximately around 3.9 s, while DNTZNN and TNTZNN accomplish this in merely 2.3 s and 0.3 s, respectively. This suggests that DNTZNN exhibits stronger noise suppression capabilities in comparison to IEZNN. Similarly, TNTZNN demonstrates enhanced noise tolerance relative to DNTZNN.

2) LINEAR NOISE

The trajectories and residual error plots of the three models addressing the TVMI problem under matrix-form time-varying linear noise are depicted in Fig. 5(a) and Fig. 5(b), respectively. The matrix-form linear noise is characterized by $N(t) = [10 + 10t]^{2\times 2}$.

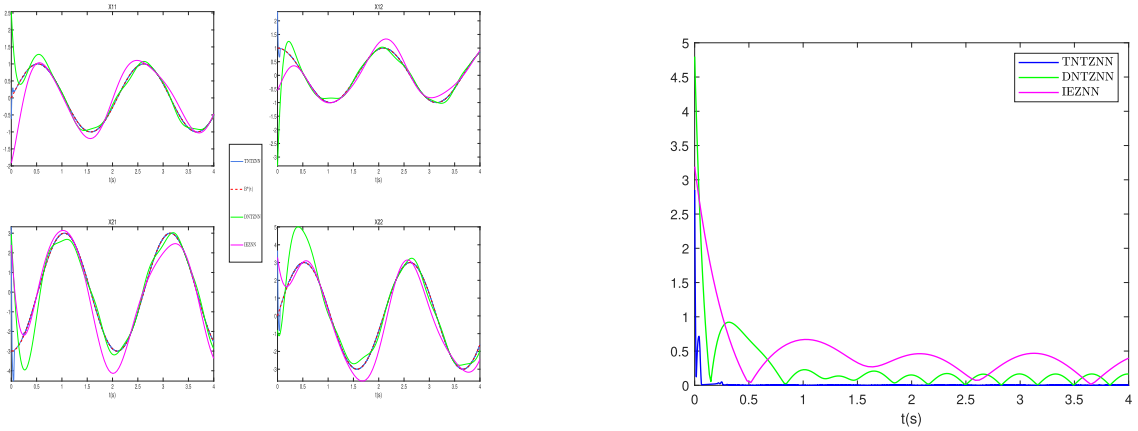

(a) Trajectory of the TNTZNN model (25) (blue solid line), DNTZNN model (10) (green solid line), and IEZNN model (8) (pink solid line) for solving the TVMI problem (66) under harmonic noise. The red dashed-dotted curves align with the theoretical inverse $B^*(t)$.

(b) Residual errors of the TNTZNN model (25) (blue solid line), DNTZNN model (10) (green solid line), and IEZNN model (8) (pink solid line) with any initial state $B(0)$ for solving the TVMI problem (66) under harmonic noise.

FIGURE 6. Robustness comparison of IEZNN, DNTZNN, and TNTZNN.

TABLE 1. Comparison of the steady-state residual error of IEZNN, DNTZNN, and TNTZNN for three different matrix-form noise types.

Model	Constant Noise $N(t) = [10]^{2\times2}$	Linear Noise $N(t) = [8+5t]^{2\times2}$	Harmonic Noise $N(t) = [1\times\sin(3\pi t+2)]^{2\times2}$
TNTZNN	Order of 10^{-4}	Order of 10^{-3}	Order of 10^{-3}
DNTZNN	Order of 10^{-4}	Order of 10^{-4}	> 0.2
IEZNN	Order of 10^{-3}	> 3	> 0.7

From the residual error plot in Fig. 5(b), it is evident that the IEZNN model fails to converge under linear noise conditions and displays considerable deviation. In contrast, both the DNTZNN and TNTZNN models achieve complete convergence to zero within 2.5 seconds and 0.3 seconds, respectively. This further underscores the inherent structural tolerance of the DNTZNN and TNTZNN models, leveraging the double integration framework to mitigate linear noise interference.

3) HARMONIC NOISE

Harmonic noise is a common type of bounded noise often encountered in real-world environments. Experimental validation demonstrates that the structure of the TNTZNN model proposed in this study inherently exhibits tolerance to harmonic noise. The computational simulation results are depicted in Fig. 6(a) and Fig. 6(b).

From Fig. 6(b), it's evident that when subjected to harmonic noise (with $N_{b1} = 3$, $N_{b0} = 1$, $N(t) = N_{b0} \times \sin(N_{b1} \times \pi \times t + 2)$), the residual error $\|A(t)B(t)-I\|_F$ of both the IEZNN and DNTZNN models fails to converge completely to zero, regardless of the initial value $B(0)$ within the range of $[-4, 4]^{2\times2}$. However, the error obtained by the DNTZNN model is notably smaller than that of the IEZNN model, indicating that the model with the double integration structure exhibits a degree of tolerance to harmonic noise interference. Furthermore, the TNTZNN model, leveraging the SBPAF activation function combined with the double integration structure, achieves complete convergence within 0.3 seconds even under harmonic noise interference. This highlights the superior tolerance of the SBPAF activation function to bounded random noise (harmonic noise), further emphasizing the inherent superiority of the proposed triple noise-tolerant ZNN model in terms of noise tolerance.

The experiments conducted highlight the significant capability of the proposed TNTZNN model in approximating the theoretical value $A^{-1}(t)$ with the computed value $B(t)$ within a relatively short time frame, even amidst various forms of noise interference. This underscores the impressive tolerance of the TNTZNN model to diverse types of noise interference when addressing the TVMI problem.

C. EXPERIMENT 3: APPLICATION ON HIGH-DIMENSIONAL COMPLEX TIME-VARYING MATRICES

To further substantiate the superiority and applicability of the proposed TNTZNN model, we simulated its performance alongside the other two ZNN models on high-dimensional time-varying Toeplitz matrix inversion. The time-varying Toeplitz matrix can be represented as follows:

$$A(t) = \begin{bmatrix} a_{11}(t) & a_{12}(t) & \dots & a_{1n}(t) \\ a_{21}(t) & a_{22}(t) & \dots & a_{2n}(t) \\ a_{31}(t) & a_{32}(t) & \dots & a_{3n}(t) \\ \vdots & \vdots & \ddots & \vdots \\ a_{n1}(t) & a_{n2}(t) & \dots & a_{nn}(t) \end{bmatrix} \in \mathbb{R}^{n\times n} \quad (70)$$

with $a_{ij}(t)$donates the ijth element-wise of $A(t)$. Thereinto

$$a_{ij}(t) = \begin{cases} n + \sin(3t), & i = j \\ \cos(3t)/(i-j), & i > j \\ \sin(3t)/(j-i), & i < j. \end{cases} \tag{71}$$

This set of experiments utilized matrices of dimension 3. For the ease of comparison and readability for readers, the noise resistance capabilities of IEZNN, DNTZNN, and TNTZNN against three different matrix-form noises, namely constant noise, time-varying linear noise, and harmonic noise, are presented in Table 1.

Clearly, for constant noise, all three models exhibit strong noise tolerance, with residual errors accurately converging to 0. However, concerning linear noise, the residual error of the IEZNN model is significantly higher, reaching the order of 3, while the residual errors of the TNTZNN and DNTZNN models both exceed the order of 10^{-3}. In terms of harmonic noise, the errors of the IEZNN and DNTZNN models reach 0.7 and 0.2, respectively, with large residuals unable to fully converge to 0. However, when using the TNTZNN model to compute the TVMI problem, the residual error reaches the order of 10^{-3}. These experiments demonstrate that even in the case of high-dimensional time-varying complex matrix inversions, TNTZNN performs well in handling various types of noise interference. This further confirms the strong tolerance of the TNTZNN model to both unbounded and bounded random noise.

VI. CONCLUSION

To address the TVMI problem under various noise disturbances more effectively, we introduced a dual integral component to the integral-enhanced zeroing neural network model, resulting in the dual noise tolerant zeroing neural network. Inspired by the noise reduction capabilities of activation functions, we incorporated a positive odd activation function into our design formula and, based on this formula, constructed and studied the novel triple noise tolerant zeroing neural network model. Using the lyapunov theorem, we rigorously analyzed and proved the convergence and robustness of the TNTZNN model against noise. We also derived its inherent structural superiority over the IEZNN model. Through quantitative comparative experiments with two different time-varying matrices, we confirmed the superior convergence of the TNTZNN model. Additionally, through three sets of comparative experiments with various types of noise, we demonstrated the model's strong tolerance to noise. Finally, by applying the TNTZNN model to the problem of inverting high-dimensional, complex, time-varying matrices under various noise conditions, we demonstrated its generalizability. Although the proposed TNTZNN model has a more complex structure, future work may include optimizing its architecture and applying it to practical engineering fields.

ACKNOWLEDGMENT

This article uses ChatGPT for syntax enhancement and polishing.

REFERENCES

[1] B. Liao, L. Han, X. Cao, S. Li, and J. Li, "Double integral-enhanced zeroing neural network with linear noise rejection for time-varying matrix inverse," *CAAI Trans. Intell. Technol.*, vol. 9, no. 1, pp. 197–210, Feb. 2024.

[2] R. Zhang, X. Xi, H. Tian, and Z. Wang, "Dynamical analysis and finite-time synchronization for a chaotic system with hidden attractor and surface equilibrium," *Axioms*, vol. 11, no. 11, p. 579, Oct. 2022.

[3] M. Z. Atwany, A. H. Sahyoun, and M. Yaqub, "Deep learning techniques for diabetic retinopathy classification: A survey," *IEEE Access*, vol. 10, pp. 28642–28655, 2022.

[4] Z. Hu, L. Xiao, K. Li, K. Li, and J. Li, "Performance analysis of nonlinear activated zeroing neural networks for time-varying matrix pseudoinversion with application," *Appl. Soft Comput.*, vol. 98, Jan. 2021, Art. no. 106735. [Online]. Available: https://www.sciencedirect.com/science/article/pii/S1568494620306736

[5] D. Guo, Z. Li, A. H. Khan, Q. Feng, and J. Cai, "Repetitive motion planning of robotic manipulators with guaranteed precision," *IEEE Trans. Ind. Informat.*, vol. 17, no. 1, pp. 356–366, Jan. 2021.

[6] B. Siciliano, L. Sciavicco, L. Villani, and G. Oriolo, *Force Control*. Heidelberg, Germany: Springer, 2009.

[7] S. Li, J. He, Y. Li, and M. U. Rafique, "Distributed recurrent neural networks for cooperative control of manipulators: A game-theoretic perspective," *IEEE Trans. Neural Netw. Learn. Syst.*, vol. 28, no. 2, pp. 415–426, Feb. 2017.

[8] Y. Wang, X. Yan, L. He, H. Tan, and Y. Zhang, "Inverse-free solution of Z1G1 type to acceleration-level inverse kinematics of redundant robot manipulators," in *Proc. 7th Int. Conf. Adv. Comput. Intell. (ICACI)*, Mar. 2015, pp. 57–62.

[9] D. F. Griffiths and D. J. Higham, *Numerical Methods for Ordinary Differential Equations: Initial Value Problems*, vol. 5. Heidelberg, Germany: Springer, 2010.

[10] H. Ramos and M. T. T. Monteiro, "A new approach based on the Newton's method to solve systems of nonlinear equations," *J. Comput. Appl. Math.*, vol. 318, pp. 3–13, Jul. 2017.

[11] Y. Zhang, "Revisit the analog computer and gradient-based neural system for matrix inversion," in *Proc. IEEE Int. Symp. Mediterrean Conf. Control Autom. Intell. Control*, Jun. 2005, pp. 1411–1416.

[12] Y. Zhang, C. Yi, D. Guo, and J. Zheng, "Comparison on Zhang neural dynamics and gradient-based neural dynamics for online solution of nonlinear time-varying equation," *Neural Comput. Appl.*, vol. 20, no. 1, pp. 1–7, Feb. 2011.

[13] L. Xiao, Y. Zhang, B. Liao, Z. Zhang, L. Ding, and L. Jin, "A velocity-level bi-criteria optimization scheme for coordinated path tracking of dual robot manipulators using recurrent neural network," *Frontiers Neurorobotics*, vol. 11, p. 47, Sep. 2017.

[14] Y. Zhang, D. Jiang, and J. Wang, "A recurrent neural network for solving Sylvester equation with time-varying coefficients," *IEEE Trans. Neural Netw.*, vol. 13, no. 5, pp. 1053–1063, Sep. 2002.

[15] Z. Sun, S. Tang, L. Jin, J. Zhang, and J. Yu, "Nonconvex activation noise-suppressing neural network for time-varying quadratic programming: Application to omnidirectional mobile manipulator," *IEEE Trans. Ind. Informat.*, vol. 19, pp. 10786–10798, 2023.

[16] Y. Zhang, W. Li, D. Guo, B. Mu, and H. Zheng, "Different Zhang functions leading to various ZNN models illustrated via solving the time-varying overdetermined system of linear equations," in *Proc. IEEE 3rd Int. Conf. Inf. Sci. Technol. (ICIST)*, Mar. 2013, pp. 771–776.

[17] L. Xiao, J. Tao, and W. Li, "An arctan-type varying-parameter ZNN for solving time-varying complex Sylvester equations in finite time," *IEEE Trans. Ind. Informat.*, vol. 18, no. 6, pp. 3651–3660, Jun. 2022.

[18] J. Dai, L. Jia, and L. Xiao, "Design and analysis of two prescribed-time and robust ZNN models with application to time-variant stein matrix equation," *IEEE Trans. Neural Netw. Learn. Syst.*, vol. 32, no. 4, pp. 1668–1677, Apr. 2021.

[19] Z. Zhang, Z. Li, and S. Yang, "A barrier varying-parameter dynamic learning network for solving time-varying quadratic programming problems with multiple constraints," *IEEE Trans. Cybern.*, vol. 52, no. 9, pp. 8781–8792, Sep. 2022.

[20] L. Xiao, Y. Zhang, J. Dai, K. Chen, S. Yang, W. Li, B. Liao, L. Ding, and J. Li, "A new noise-tolerant and predefined-time ZNN model for time-dependent matrix inversion," *Neural Netw.*, vol. 117, pp. 124–134, Sep. 2019.

[21] L. Xiao, Y. Zhang, J. Dai, J. Li, and W. Li, "New noise-tolerant ZNN models with predefined-time convergence for time-variant Sylvester equation solving," *IEEE Trans. Syst., Man, Cybern., Syst.*, vol. 51, no. 6, pp. 3629–3640, Jun. 2021.
[22] Z. Zhang, X. Deng, X. Qu, B. Liao, L.-D. Kong, and L. Li, "A varying-gain recurrent neural network and its application to solving online time-varying matrix equation," *IEEE Access*, vol. 6, pp. 77940–77952, 2018.
[23] Z. Tan, W. Li, L. Xiao, and Y. Hu, "New varying-parameter ZNN models with finite-time convergence and noise suppression for time-varying matrix Moore–Penrose inversion," *IEEE Trans. Neural Netw. Learn. Syst.*, vol. 31, no. 8, pp. 2980–2992, Aug. 2020.
[24] M. Zheng, L. Li, H. Peng, J. Xiao, Y. Yang, and H. Zhao, "Parameters estimation and synchronization of uncertain coupling recurrent dynamical neural networks with time-varying delays based on adaptive control," *Neural Comput. Appl.*, vol. 30, no. 7, pp. 2217–2227, Oct. 2018.
[25] D. Guo, S. Li, and P. S. Stanimirovic, "Analysis and application of modified ZNN design with robustness against harmonic noise," *IEEE Trans. Ind. Informat.*, vol. 16, no. 7, pp. 4627–4638, Jul. 2020.
[26] L. Jin, Y. Zhang, and S. Li, "Integration-enhanced Zhang neural network for real-time-varying matrix inversion in the presence of various kinds of noises," *IEEE Trans. Neural Netw. Learn. Syst.*, vol. 27, no. 12, pp. 2615–2627, Dec. 2016.
[27] L. Jin, S. Li, L. Xiao, R. Lu, and B. Liao, "Cooperative motion generation in a distributed network of redundant robot manipulators with noises," *IEEE Trans. Syst., Man, Cybern., Syst.*, vol. 48, no. 10, pp. 1715–1724, Oct. 2018.
[28] L. Jin, S. Li, B. Hu, M. Liu, and J. Yu, "A noise-suppressing neural algorithm for solving the time-varying system of linear equations: A control-based approach," *IEEE Trans. Ind. Informat.*, vol. 15, no. 1, pp. 236–246, Jan. 2019.
[29] M. A. Johnson and M. H. Moradi, *PID Control*. Heidelberg, Germany: Springer, 2005.
[30] L. Han, B. Liao, Y. He, and X. Xiao, "Dual noise-suppressed ZNN with predefined-time convergence and its application in matrix inversion," in *Proc. 11th Int. Conf. Intell. Control Inf. Process. (ICICIP)*, Dec. 2021, pp. 410–415.
[31] L. Xiao, Y. He, J. Dai, X. Liu, B. Liao, and H. Tan, "A variable-parameter noise-tolerant zeroing neural network for time-variant matrix inversion with guaranteed robustness," *IEEE Trans. Neural Netw. Learn. Syst.*, vol. 33, no. 4, pp. 1535–1545, Apr. 2022.
[32] S. Li, S. Chen, and B. Liu, "Accelerating a recurrent neural network to finite-time convergence for solving time-varying Sylvester equation by using a sign-bi-power activation function," *Neural Process. Lett.*, vol. 37, no. 2, pp. 189–205, Apr. 2013.
[33] X. Lan, J. Jin, and H. Liu, "Towards non-linearly activated ZNN model for constrained manipulator trajectory tracking," *Frontiers Phys.*, vol. 11, Mar. 2023, Art. no. 1159212.
[34] L. Xiao, Y. Zhang, K. Li, B. Liao, and Z. Tan, "A novel recurrent neural network and its finite-time solution to time-varying complex matrix inversion," *Neurocomputing*, vol. 331, pp. 483–492, Feb. 2019.
[35] L. Xiao, "A nonlinearly activated neural dynamics and its finite-time solution to time-varying nonlinear equation," *Neurocomputing*, vol. 173, pp. 1983–1988, Jan. 2016.
[36] Y. Yang and Y. Zhang, "Superior robustness of power-sum activation functions in Zhang neural networks for time-varying quadratic programs perturbed with large implementation errors," *Neural Comput. Appl.*, vol. 22, no. 1, pp. 175–185, Jan. 2013.

FEIXIANG YANG has been with the College of Computer Science and Engineering, Jishou University, Jishou, China, since 2021. His major is software engineering. His current research interest includes neural networks.

YUN HUANG received the Ph.D. degree in computer software and theory from Sun Yat-sen University, Guangzhou, China, in 2017. He is currently an Associate Professor with the College of Computer Science and Engineering, Jishou University. He has published more than 20 papers in various journals/conferences. His current research interests include neural networks and graph processing.